Chemical Science

ROYAL SOCIETY OF CHEMISTRY

EDGE ARTICLE

View Article Online
View Journal | View Issue

Cite this: *Chem. Sci.*, 2023, **14**, 2369

All publication charges for this article have been paid for by the Royal Society of Chemistry

Received 21st November 2022
Accepted 3rd February 2023

DOI: 10.1039/d2sc06413h

rsc.li/chemical-science

A tumor-targetable NIR probe with photoaffinity crosslinking characteristics for enhanced imaging-guided cancer phototherapy†

Rui Sun,‡ Yuqi Zhang,‡ Yinjia Gao, Meng Zhao, Anna Wang, Jinfeng Zhu, Xiaju Cheng* and Haibin Shi *

Spatiotemporally manipulating the *in situ* immobilization of theranostic agents within cancer cells to improve their bioavailability is highly significant yet challenging in tumor diagnosis and treatment. Herein, as a proof-of concept, we for the first time report a tumor-targetable near-infrared (NIR) probe DACF with photoaffinity crosslinking characteristics for enhanced tumor imaging and therapeutic applications. This probe possesses great tumor-targeting capability, intensive NIR/photoacoustic (PA) signals, and a predominant photothermal effect, allowing for sensitive imaging and effective photothermal therapy (PTT) of tumors. Most notably, upon 405 nm laser illumination, DACF could be covalently immobilized within tumor cells through a photocrosslinking reaction between photolabile diazirine groups and surrounding biomolecules resulting in enhanced tumor accumulation and prolonged retention simultaneously, which significantly facilitates the imaging and PTT efficacy of tumor *in vivo*. We therefore believe that our current approach would provide a new insight for achieving precise cancer theranostics.

Introduction

A molecule imaging probe, as a fascinating tool for precise cancer diagnosis and treatment, has drawn considerable attention over the past few decades due to its great capacity to accurately detect and visualize the behavior of cancer-related biomarkers in living subjects.[1–6] As an outstanding representative, a small molecule probe (SMP) shows great potential for clinical applications due to its unique advantages, such as facile synthesis, noninvasiveness, rapid metabolism, and excellent biocompatibility.[7–15] Thus far, a large number of SMPs were developed for cancer imaging and therapeutic applications. For instance, indocyanine green (ICG), an USA Food and Drug Administration (FDA) approved NIR fluorescent agent, has been widely utilized in clinical diagnostic applications and acknowledged as a promising photothermal therapeutic agent.[16–18] Nevertheless, the low theranostic efficacy of many SMPs owing to poor tumor specificity, insufficient accumulation, and rapid renal excretion impedes their extensive application in clinics. Therefore, it is highly meaningful to exploit novel strategies that enable the conventional probes to be efficiently and on-demand immobilized at targeted sites resulting in enhanced accumulation and prolonged retention for effective cancer theranostics.

Over the past few decades, in an attempt to improve cancer diagnostic and therapeutic outcomes, tremendous efforts have been devoted to promoting the enrichment of theranostic agents within tumors through passive targeting based on the EPR effect,[19–22] long-term blood circulation,[23] and active targeting using specific ligands (*e.g.* antibodies, peptides, and folic acid[24–26]) that can significantly improve the ligand-receptor binding affinity. Recently, a stimulus-responsive strategy has aroused increasing interest for locally inducing self-assembly of small molecules to form nanostructures at tumorous sites under specific physiological or pathological environments.[27–33] Xu and co-workers developed an enzyme-mediated self-assembly approach that induces small molecules to specifically form a hydrogel within cancer cells leading to enhanced cellular uptake and retention.[34,35] Alternatively, Rao and Liang exploited a bioorthogonal cyclization reaction between 2-cyanobenzothiazole (CBT) and 1,2-aminothiol to achieve the self-assembly of small molecules for *in vivo* imaging enzyme activity.[36–40] Wang and co-workers reported an *in situ* morphology-defined self-assembly approach that exhibits the

State Key Laboratory of Radiation Medicine and Protection, School for Radiological and Interdisciplinary Sciences (RAD-X) and Collaborative Innovation Center of Radiation Medicine of Jiangsu Higher Education Institutions, Soochow University, Suzhou 215123, P. R. China. E-mail: xjcheng@suda.edu.cn; hbshi@suda.edu.cn

† Electronic supplementary information (ESI) available: Experimental details and results of the structural characterization of compounds **1**, **2**, **3**, **4**, **5**, **1′**, **2′**, DACF, and CF; fluorescence intensities of the tumors; *ex vivo* fluorescence images and CLSM images of tumorous tissues; photothermal conversion efficiency (η) of DACF; photothermal images of 4T1 cells; apoptosis rates of 4T1 cells with various treatments; hyperthermia heating curves of the tumors; representative tumor and lung images from different groups of mice. See DOI: https://doi.org/10.1039/d2sc06413h

‡ Rui Sun and Yuqi Zhang contributed equally to this work.

assembly induced retention (AIR) effect and can dramatically improve the bioavailability and treatment outcome of small molecules in tumor theranostics.[41–44] In spite of the evident improvement achieved, these strategies based on self-assembly unavoidably suffer from unwanted particle aggregation and significant entrapment by the reticuloendothelial system (RES) after systemic administration. Recently, a cell-membrane anchoring approach based on the hydrophobic interaction between the lipophilic tail of biosensors and cellular phospholipid layer was employed for real-time monitoring of pH,[45,46] metal ions,[47] carbon monoxide release,[48] and cancer-associated enzyme's activity[49,50] in the cellular microenvironment. However, the non-covalent binding between probes and targets only provides limited imaging and therapeutic efficacy. Herein, we for the first time propose to develop a photochemical strategy capable of manipulating the on-site immobilization of theranostic agents under light stimulation so as to improve their accumulation and retention in tumors for effective theranostics. As a matter of fact, light is well documented as a promising and controllable external stimulus that has been extensively applied in various biomedical applications because of simplicity, low cost, spatiotemporal addressability, and minimal invasiveness.[51–54] The photocrosslinking technique as an effective tool for covalent attachment of molecules onto their targets has drawn great attention in biological applications over the decades. Although various types of photo-crosslinkers have been used for studying the intermolecular interactions of drug-targets,[55,56] protein–protein/DNA interactions,[57,58] *etc*,[59–63] to our knowledge utilizing this approach to spatiotemporally enhance the accumulation and retention of theranostic agents within cancer cells or tumor tissues has rarely been reported thus far.

In this study, we rationally designed and synthesized a tumor-targetable NIR probe DACF with photoaffinity crosslinking characteristics for prolonged NIR/PA dual modality imaging and enhanced PTT applications of tumors *in vivo*. As illustrated in Scheme 1, the probe DACF consists of NIR dye cypate, a derivative of ICG, as the signal unit, folic acid (FA) as the tumor targeting ligand, and a photolabile diazirine (DA) that can be initiated by 405 nm irradiation to generate reactive carbene intermediates followed by the formation of covalent bonds with adjacent biomolecules through C–C, C–H, O–H, and X–H (X = heteroatom) insertion reactions,[64–66] leading to the immobilization of probes in tumor. Taking advantage of the active targeting and *in situ* immobilization, such a strategy may provide a promising means to improve the accumulation and prolong the retention of therapeutic agents for enhanced imaging-guided PTT of tumors *in vivo*.

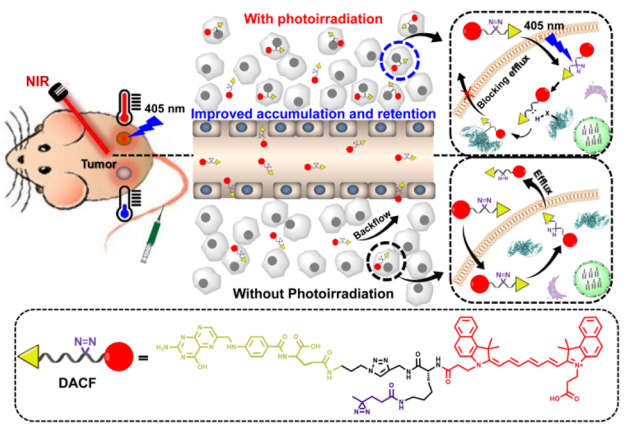

Scheme 1 A tumor-targetable NIR probe DACF with photoaffinity crosslinking characteristics for enhanced imaging-guided photothermal therapy of tumors.

Results and discussion

The probe DACF was synthesized according to the synthetic route shown in Scheme S1 in the ESI.† Briefly, Fmoc-Lys(Boc)-COOH was first reacted with 2-propynylamine through the amidation reaction between carboxylic acid and amine groups to afford compound **1**. Next, the Boc group on the side chain of **2** was deprotected under acidic conditions followed by acylation with NHS-diazirine to give **3**. The subsequent Fmoc deprotection yielded the corresponding amine **4**, which was further reacted with a dicarboxylic acid-containing carbocyanine analog (Cypate) to afford **5**. Azido-functionalized folic acid (FA-N_3) was eventually conjugated to compound **5** in a DMSO/water (1 : 1 by vol) mixture by a copper(I)-catalyzed "click" reaction followed by purification *via* HPLC to obtain the desired probe DACF in total 26.7% yield. The intermediates and DACF were characterized by nuclear magnetic resonance (NMR) and high-resolution mass spectrometry (HR-MS) (Fig. S1–S13†). Meanwhile, one control probe CF that does not contain the diazirine group was also synthesized and confirmed by both NMR and HR-MS (Scheme S2 and Fig. S14–S18†).

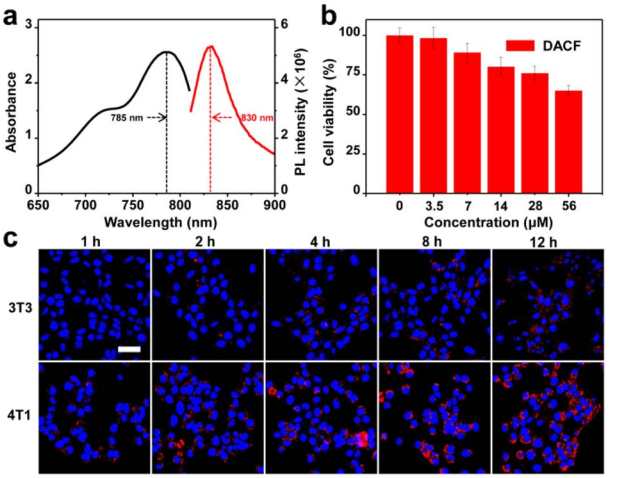

Fig. 1 *In vitro* characterization of the probe DACF. (a) UV-vis absorption and fluorescence spectra of DACF (4 μM) in DMSO solution. λ_{ex} = 785 nm and λ_{em} = 830 nm. (b) MTT assays on the viability of 4T1 cells after being incubated with the different concentrations of DACF, *i.e.* 0, 3.5, 7, 14, 28, and 56 μM for 24 h (the error bars represent the standard deviations of six parallel measurements). (c) CLSM images of 3T3 and 4T1 cells after incubation with DACF (1 μM) for 1, 2, 4, 8, and 12 h. $\lambda_{ex/em}$ = 635/(710 ± 50) nm. The embedded scale bar corresponds to 30 μm.

Our first step was to investigate the optical properties of the probe DACF. Fig. 1a shows the absorption and NIRF spectra of DACF in DMSO solution. DACF intrinsically has an absorption maximum at 785 nm and is highly fluorescent at 830 nm with a fluorescence quantum yield of around 0.48, implying that this probe has the capability of *in vivo* deep-tissue and sensitive bioimaging. To evaluate the photocrosslinking capability of DACF to proteins in aqueous solution, bovine serum albumin (BSA) as a model protein was mixed with the probe DACF and control CF, respectively, and then exposed to 405 nm laser light followed by gel electrophoresis. The BSA protein in the assays with the treatment of DACF and 405 nm showed obviously strong fluorescence in a concentration-dependent manner, while almost no fluorescence was detected for the assays receiving CF and 405 nm (Fig. S19†), demonstrating that proteins can be covalently labeled with DACF under the irradiation of 405 nm laser light. Next, to explore the potential biomedical application of DACF in living systems, the cytotoxicity of DACF was evaluated through the widely used methyl thiazolyl tetrazolium (MTT) assay with mouse mammary carcinoma cells 4T1. The overall cell viability remained 80.1% after being incubated with the probes up to 14 μM for 24 h (Fig. 1b), indicative of negligible cytotoxicity of DACF towards 4T1 cells. In the subsequent experiments, the concentration of DACF used is essentially much lower than 14 μM. To investigate the specificity of DACF toward cancer cells, a 4T1 cell was chosen as the folic acid receptor over-expressed cancer cell, while a mouse normal embryo fibroblast 3T3 cell with a low level of folic acid receptor was used as a negative control. Confocal laser scanning microscopy (CLSM) was employed to image the cells at selected time points after being incubated with 1 μM DACF. No autofluorescence signals were detected from the cells themselves under identical experimental condition. As shown in Fig. 1c, 4T1 cells obviously show stronger NIR fluorescence than 3T3 cells at the recorded time points. Moreover, as the incubation time elapsed, the fluorescence intensity of the 4T1 cells treated with DACF increased gradually. These results indicate that DACF is undoubtedly a specific probe for folic acid receptor-overexpressed cancer cells.

To investigate whether this *in situ* covalent photocrosslinking approach can alleviate the diffusing of probes from living cells, an *in vitro* NIR imaging experiment was first performed and the cellular uptake of DACF in 4T1 cells was evaluated by CLSM. Two groups of cells were treated with 1 μM DACF, respectively. After 12 h incubation, one group of cells was exposed to a 405 nm laser (1 W cm^{-2}, 1.5 min) followed by continuously monitoring the fluorescence signals of the cells. The NIRF intensities of the two groups of cells were measured to be nearly identical at the initial stage. The fluorescence of the cells without photo-irradiation rapidly faded over time, while the cells with the photo-crosslinking process kept strong fluorescence for a long time (Fig. 2a), which was further confirmed by the quantitative results in Fig. 2b. The cells with photo-irradiation retain *ca.* 10.9% of the initial fluorescence signals after 48 h of further incubation. In sharp contrast, only ~0.6% of the initial signal is preserved for the cells without

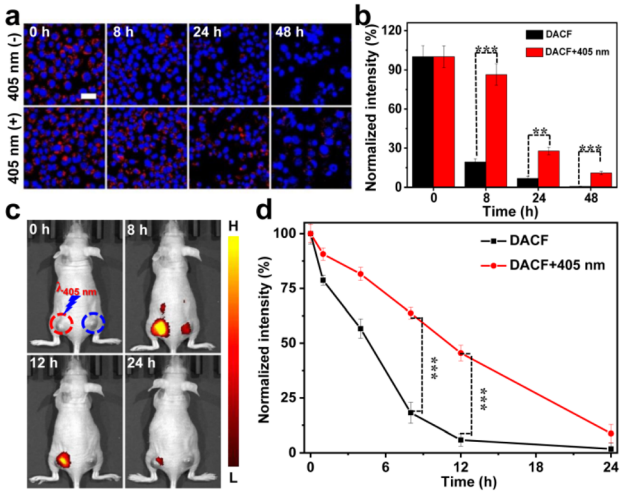

Fig. 2 Bioimaging performance evaluation of the probe DACF. (a) Confocal imaging and (b) normalized fluorescent intensity of DACF-treated 4T1 cells before (top) and after (bottom) 405 nm laser irradiation at 0, 8, 24, and 48 h. Condition: 4T1 cells were incubated with DACF (1 μM) for 12 h followed by 405 nm laser irradiation (1 W cm^{-2} and 1.5 min). $\lambda_{ex/em} = 635/(710 \pm 50)$ nm. All images share the same scale bar (30 μm). (c) *In vivo* fluorescence images and (d) normalized fluorescent intensity of 4T1 tumor-bearing nude mice receiving DACF (200 μL, 45 μM) with (left tumor) and without (right tumor) 405 nm irradiation (1 W cm^{-2} and 10 min) at 0, 8, 24, and 48 h. $\lambda_{ex/em} = 745/(815 \pm 25)$ nm (exposure time: 200 ms). The circles point the tumor locations in mice. Data denote mean ± SD ($n = 3$, $^{**}P < 0.01$, and $^{***}P < 0.001$).

photo-illumination. This could be probably due to the photo-crosslinking between probes and the surrounding biomolecules, which can effectively prolong the residence time of probes in cancer cells. However, for the control probe CF, the fluorescence of the cells gradually decayed in a similar way whether the cells were treated with or without 405 nm laser irradiation (Fig. S20†). Together, all these results highly demonstrated that the probe DACF has great potential for long-term cancer cell imaging.

Inspired by the above exciting results, we next investigated the light-initiated *in situ* crosslinking effect of DACF *in vivo*. We first optimized the irradiation time of the 405 nm laser for *in vivo* photoaffinity crosslinking. 10 min illumination of the 405 nm laser (1 W cm^{-2}) on tumors was eventually chosen as the optimal irradiation condition (Fig. S21†). The tumor targeting specificity and photo-crosslinking performance of the probes in 4T1 cell xenografted BALB/c mice were then evaluated. The mice were intravenously administered with DACF at a dosage (200 μL, 45 μM) *via* the tail vein. Increased fluorescence signals at the tumor site were clearly recorded, and the maximum signal intensity was reached approximately 0.5 h post injection, indicating that DACF is a specific probe for *in vivo* tumor imaging (Fig. S22†). To assess the capability of DACF for enhanced accumulation and retention within tumor tissues, 200 μL of DACF aqueous solution (45 μM) was intravenously injected into two 4T1 tumors bearing mice on both left and right sides of the back. At 0.5 h post injection, the tumors on the left side of the mice were exposed to a 405 nm laser (1 W cm^{-2})

for 10 min followed by NIRF imaging. Consistent with the aforementioned cell imaging results, the tumors on the left side of the mice obviously exhibited stronger fluorescence than the right side of tumors at each recorded time point (8, 12 and 24 h) (Fig. 2c). Quantitative analysis indicated that the left side of tumors receiving DACF at 24 h still retained 8.8% NIRF signals of that at 0.5 h. However, it was only 1.8% for the right side of tumors (Fig. 2d), suggesting that DACF has poor retention in the tumor region if no photo-irradiation was applied. This was also directly proved by the *ex vivo* fluorescence images of dissected organs as well as tumorous tissue sections (Fig. S23 and S24†). Meanwhile, the control probe CF was intravenously injected into two tumor-bearing mice and the left tumor was exposed to a 405 nm laser followed by fluorescence imaging. Fig. S25† shows that the fluorescence signals of both two tumors rapidly decayed following the same trend. Collectively, these results strongly demonstrate that the *in situ* covalent photo-crosslinking of the probes could take place *in vivo*.

The absorption profile of the probe DACF in aqueous solution was also obtained. As shown in Fig. 3a, broad absorption in the NIR region of 700–900 nm is apparently observed, implying that DACF may be useful for PAI and PTT applications. To demonstrate our hypothesis, the PAI signals of various concentrations of DACF aqueous solutions were measured. As expected, intensive PA signals were recorded at 680 nm for DACF aqueous solutions. This is probably ascribed to its strong NIR absorption. Additionally, the PA signals linearly increased with the increasing concentration of DACF from 0 to 4.8 μM (Fig. 3b), suggesting that DACF may be a promising contrast agent for PA imaging. The *in vivo* PA imaging performance of DACF was further evaluated in two subcutaneous 4T1 tumor-bearing mice. At 0.5 h post injection of DACF into mice through the tail vein, the tumors on the left back of the mice were exposed to a 405 nm laser (1 W cm^{-2}) for 10 min followed by real-time PA imaging under 680 nm illumination. As expected, the PA signals of both tumors were initially almost identical whether they were treated with photoirradiation or not. However, gradual decay of PA intensity with time was observed for both tumors. In contrast, the PA intensity of the right tumor decreased rapidly, which should be attributed to the quick efflux of the probes from the tumor. Besides, the PA signals on the left tumor were obviously higher than that of the right one at each recorded time point (Fig. 3c). The quantitative data further indicate that the left tumor retains 12.5% PA signals of that at the beginning even after 24 h, whereas only 1.9% is retained for the right tumor (Fig. 3d). This evidence strongly demonstrates that the light-initiated immobilization of DACF can significantly prolong the residence time of probes in tumors.

Furthermore, to investigate the PTT effect of DACF, different concentrations of DACF aqueous solutions were continuously irradiated with an 808 nm laser (1.0 W cm^{-2}) for 300 s, and their temperature elevation was monitored by using an infrared camera. As shown in Fig. 4a, the aqueous solution containing DACF presented a large temperature rise with increasing concentration and irradiation time. For instance, the temperature of DACF solution (4 μM) increased ~17.2 °C after 808 nm laser irradiation (1.0 W cm^{-2} and 5 min). The photothermal conversion efficiency (η%) was calculated to be ~11.3% for DACF (Fig. S26†). These results firmly imply that DACF has good photothermal conversion efficiency. The photothermal stability of the probe was further assessed. DACF solution was irradiated at 808 nm for 5 min and then cooled to room temperature. After 3 repeated cycles, good consistency of temperature changes was observed (Fig. 4b), indicating that it

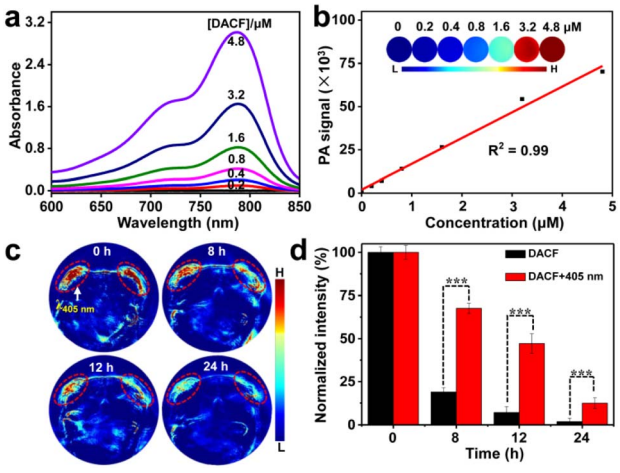

Fig. 3 Photoacoustic properties of DACF. (a) UV-vis absorption spectra and (b) PA signal of DACF aqueous solutions with different concentrations (0, 0.2, 0.4, 0.8, 1.6, 3.2 and 4.8 μM). (c) *In vivo* PA imaging and (d) normalized PA signal of 4T1 tumor-bearing nude mice at 0, 8, 12 and 24 h after 405 nm irradiation. Left tumor was exposed to a 405 nm laser (1 W cm^{-2}) for 10 min at 0.5 h post injection of DACF (45 μM, 200 μL). The photoacoustic images and signal of the tumor site recorded under illumination at 680 nm. Red circles point the tumor locations in mice. Data denote mean ± SD (n = 3 and ***P < 0.001).

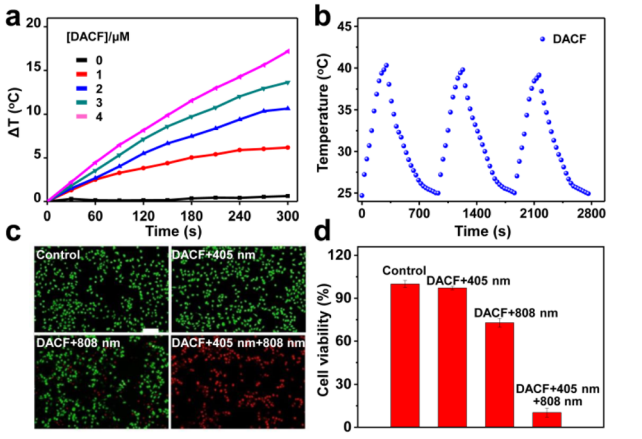

Fig. 4 Photothermal properties of DACF *in vitro*. (a) Time-dependent temperature increase curves with different concentrations of DACF (0, 1, 2, 3 and 4 μM) upon 808 nm irradiation (1 W cm^{-2}). (b) Temperature changes of DACF aqueous solution (4 μM) over several ON/OFF cycles upon 808 nm laser irradiation (1 W cm^{-2}) for 5 min followed by passive cooling. (c) Fluorescence images (stained with the live/dead kit) and (d) viability of 4T1 cells with various treatments (control, DACF + $\lambda_{405\ nm}$, DACF + $\lambda_{808\ nm}$, and DACF + $\lambda_{405\ nm}$ + $\lambda_{808\ nm}$). 405 nm laser: 1 W cm^{-2}. 808 nm laser: 3 W cm^{-2}. All images share the same scale bar (100 μm).

has excellent photostability under NIR irradiation. Together, these results firmly demonstrate that DACF has great photothermal conversion efficiency.

The photothermal ablation effect of DACF on 4T1 cells was then characterized through live/dead assays. 4T1 cells receiving DACF and 405 nm irradiation followed by 808 nm laser irradiation (DACF + 405 nm + 808 nm) were the experimental group, while the cells receiving physiological saline (control), DACF followed by 405 nm laser irradiation (DACF + 405 nm), and DACF followed by 808 nm laser irradiation (DACF + 808 nm) were set as control groups. The results in Fig. 4c and S27† indicate that effective cell thermal ablation was achieved for DACF + 405 nm + 808 nm. In sharp contrast, no evident influence on the cell viability of all three control groups was determined, which was further verified by the quantified results obtained through MTT and flow cytometry (Fig. 4d and S28†). Collectively, these experimental results firmly demonstrate that DACF is a potential photothermal agent for cancer photothermal therapy, and the enhanced PTT capability endowed by the light-initiated immobilization effect probably makes DACF promising for tumor theranostics.

To investigate the bioavailability of DACF for tumor photothermal therapy *in vivo*, two groups of 4T1 tumor-bearing mice ($n = 5$) were treated with the same amount of DACF intravenously. At 0.5 h post injection, one group of tumors was exposed to 405 nm laser light (1 W cm^{-2}) for 10 min followed by 808 nm irradiation (1 W cm^{-2} and 5 min) as the experimental group. The other one without 405 nm irradiation is set as the control group. As shown in Fig. 5a, the temperature of tumors with photo-crosslinking increased to 53.2 °C, which is high enough to ablate the tumor cells. However, a temperature increase of only 9.7 °C was determined for the control tumor upon the same dose of NIR irradiation (Fig. S29†). To further investigate the photothermal ablation effect *in vivo*, the tumor sizes of four groups of 4T1 tumor-bearing BALB/c mice receiving physiological saline (control), DACF followed by 405 nm laser irradiation (DACF + 405 nm), DACF followed by 808 nm laser irradiation (DACF + 808 nm), and DACF followed by 405 nm and 808 nm laser irradiation (DACF + 405 nm + 808 nm) were measured over 30 days. As shown in Fig. 5b and c, the tumor size dramatically increases in a similar way for control, DACF + 405 nm and DACF + 808 nm groups. In huge contrast, the tumors of the DACF + 405 nm + 808 nm group were completely eliminated after 30 days (Fig. S30†). The survival rates of mice with different treatments are given in Fig. 5d. In comparison with control groups, the DACF + 405 nm + 808 nm group shows a great survival rate, and no single death occurred over 30 days. To assess the PTT efficacy, the tumorous tissues were extracted 3 days post treatment and subjected to hematoxylin and eosin (H&E) staining. Compared to the control groups, severe necrosis was observed from the experimental group (Fig. 5e), which indicates the excellent PTT efficacy of DACF if the photo-crosslinking process was applied. In addition, no obvious body weight loss during 30 day treatment was observed from all the mice (Fig. S31†). Moreover, the H&E staining images of major organs (heart, liver, spleen, lungs, and kidneys) collected from the experimental group showed that neither obvious damage nor lung metastasis was observed compared to the control groups (Fig. S32 and S33†). To evaluate the biological safety of DACF, blood routine and blood chemical analysis were further performed for the mice receiving single intravenous injection of saline (control) or DACF after 1, 7, and 18 days. As shown in Fig. S34,† no apparent damage to the liver and kidneys was determined. Together, all these results strongly demonstrate that this light-initiated *in situ* crosslinking approach could effectively enhance the imaging-guided PTT efficacy of tumors in living systems.

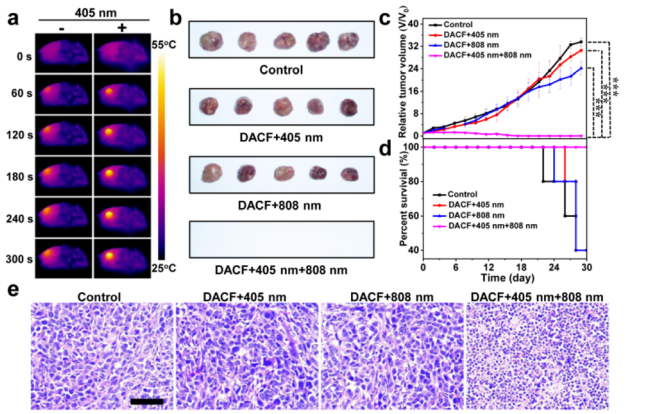

Fig. 5 *In vivo* photothermal therapy of tumors. (a) Infrared thermal images of the tumorous sites in mice injected intravenously with DACF (90 μM, 200 μL) against 808 nm laser irradiation after 8 h of 405 nm laser irradiation. (b) Photographs of tumors harvested from mice receiving different treatments on 30th day. (c) Variation of the tumor volume (normalized to their initial volumes) and (d) survival rate of mice receiving different treatments ($n = 5$). (e) Slices of tumor tissues extracted on the third posttreatment stained with hematoxylin and eosin (H&E). 808 nm irradiation: 1 W cm^{-2}. All images share the same scale bar (50 μm). Data denote mean ± SD ($n = 5$ and $^{***}P < 0.001$).

Conclusion

In summary, we have successfully developed a novel tumor-targetable and photocrosslinkable NIR small molecule probe that can be initiated with 405 nm light to form a covalent bond with the surrounding biomolecules in tumors resulting in improved tumor accumulation as well as prolonged retention simultaneously, which has been demonstrated to significantly improve the efficacy of NIRF/PAI dual-modality imaging and photothermal therapy of tumors *in vivo*. We thus believe that the delicate light-initiated *in situ* crosslinking concept would offer a new insight for effective cancer theranostics.

Experimental section

General information

A MTT cell proliferation cytotoxicity assay kit was obtained from Sigma Aldrich (St. Louis, MO). Hoechst 33342 was purchased from BD (Franklin, NJ). A live/dead cell staining kit (calcein-AM-propidium iodide) from Invitrogen (Carlsbad, CA) and an apoptosis detection kit (Annexin V-PE/7-AAD) from BD (Franklin, NJ) were used as received. All chemical reagents used

in the synthesis of the probe were obtained from Sigma Aldrich (St. Louis, MO) and used without any further purification. MilliQ water with a resistivity above 18 MΩ cm was used in the experiments.

HPLC profiles were acquired using a 1260 high performance liquid chromatograph (Agilent). HR-MS was performed on a 6230 time-of-flight mass spectrometer and 6540 UHD accurate-mass quadrupole time-of-flight mass spectrometer (Agilent). The ^{1}H and ^{13}C NMR spectra were acquired on a 400 MHz Bruker Avance III 400 spectrometer (Bruker). UV-vis absorption spectra were recorded on a UV spectrometer (UV-3600, Shimadzu). Fluorescence spectra were recorded on a fluorescence spectrometer (FLS980, Edinburgh). The absorbance was measured using an EnSpire® multimode plate reader (PerkinElmer). The fluorescence images of the probe and mice were acquired with an IVIS® spectrum *in vivo* imaging system (PerkinElmer). The fluorescence micrographs were captured with a fluorescence microscope (FV1200, Olympus). PA imaging was performed with a multispectral optoacoustic tomography (MSOT) scanner (iThera Medical). CW laser diodes with output wavelengths at 405 nm and 808 nm were used for the crosslinking of DACF and photothermal therapy (Hi-Tech Optoelectronics Co., Ltd Beijing, China).

Synthesis, purification and characterization of the probe DACF

For the synthesis of DACF, compound **5** (9 mg, 0.01 mmol) was first dissolved in 0.5 mL of DMSO and then introduced into 0.5 mL of aqueous solution containing 4.93 mg of FA-N_3 (5.2 mg, 0.01 mmol), $CuSO_4$ (0.09 mg, 0.0005 mmol), and sodium ascorbate (00.2 mg, 0.001 mmol). The mixture was stirred at room temperature for 8 h and monitored by HPLC. The reaction was finally purified by prep-HPLC using MeCN and H_2O containing 0.1% TFA as eluents to afford DACF as (12.8 mg, 94%) cyanic solid powder followed by the characterization of HR-MS. Calcd for $C_{77}H_{87}N_{18}O_{10}^{+}$, ($[M]^{+}$): 1423.6847, found HR-MS: m/z 1423.1622.

Photothermal effect, photostability, and photothermal conversion efficiency

A series of DACF aqueous solutions with the concentrations of 0, 1, 2, 3, and 4 μM were irradiated with an 808 nm laser, and their temperatures were determined with an infrared thermal imaging camera (FLIR, A65). The photostability of DACF was estimated by irradiating 4 μM solutions in a quartz cuvette with an 808 nm laser (1 W cm^{-2}) for 5 min (laser on) and then cooling to room temperature without irradiation (laser off). Such heating/cooling processes were repeated three times to test the photostability.

To determine the photothermal conversion efficiency (η) of DACF, 4 μM DACF solution was continuously irradiated with an 808 nm laser (1 W cm^{-2}) to reach a steady temperature, and the laser was then turned off to allow the solution to naturally cool to room temperature. The photothermal conversion efficiency (η) was calculated with the following equation: $\eta = mc(T_{max} - T_{max}, H_2O)/(I(1 - 10 - A)\tau_s)$, where m is the solution mass, c is the heat capacity of water (4.2 J g^{-1}), T_{max} and T_{max}, H_2O are the maximum temperatures achieved in the presence or absence of DACF, respectively, I is the laser power density (1 W cm^{-2}), A is the absorbance of DACF solution at 808 nm, and τ_s is the system time constant.

In vitro PA imaging

PA imaging was performed with a Multispectral Optoacoustic Tomography scanner (MSOT, iThera medical, Germany) with excitation light of 680–800 nm. Various concentrations of DACF (0, 0.2, 0.4, 0.8, 1.6, 3.2, and 4.8 μM) in aqueous solutions were determined on a MSOT with excitation light of 680–800 nm.

Cell culture

The murine breast carcinoma cell line 4T1 and murine embryonic fibroblast cell line 3T3 were acquired from the Cell Bank of the Chinese Academy of Sciences. 4T1 cells were cultured in RPMI 1640 medium (Hyclone Inc.), supplemented with 10% fetal bovine serum (Hyclone Inc.) and 1% penicillin streptomycin (Beyotime Inc.), at 37 °C in a humidified atmosphere of 5% CO_2. 3T3 cells were cultured in DMEM medium (Hyclone Inc.), supplemented with 10% fetal bovine serum (Hyclone Inc.) and 1% penicillin streptomycin (Beyotime Inc.), at 37 °C in a humidified atmosphere of 5% CO_2. The cells were cultured until 75% confluence was reached, and experiments were performed.

Cytotoxicity assay

The cytotoxicity of DACF was measured using commonly by using MTT assay. 4T1 cells were planted at a density of 1×10^4 cells per well in a 96-well cell culture plate. After growing for 24 h, the cells were incubated with different concentrations of DACF (0, 3.5, 7, 14, 28, and 56 μM). Then, the cell viability was determined by using the MTT cell proliferation cytotoxicity assay kit 24 h post-treatment. The absorbance was measured using an EnSpire multimode plate reader at a wavelength of 490 nm.

In vitro BSA labeling

BSA (2.5 mg mL^{-1}) was mixed with different concentrations of DACF or CF (0, 250, and 500 μM) in a total volume of 50 μL PBS buffer. The mixture was then irradiated with 405 nm laser light (1 W cm^{-2}) for 15 min, and then diluted with 4× SDS sample buffer for separation by using 10% SDS-PAGE gel.

Confocal imaging

4T1 and 3T3 cells were plated in 8-well plates with a concentration of 1×10^4 cells per well, respectively. After growing for 24 h, both cells were incubated with DACF (200 μL, 1 μM). Then, cell fluorescence imaging was performed by using a Hoechst 33342 assay kit at selected time points (1, 2, 4, 8, and 12 h) after the treatments. The samples were imaged through an FV1200 laser scanning confocal microscope. To investigate the photo-crosslinking ability of DACF in living cells, 4T1 cells were plated in 8-well plates with a concentration of 1×10^4 cells per

well. After growing for 24 h, the cells were incubated with 200 μL of DACF or CF (1 μM). After 12 h incubation, one group of cells was exposed to a 405 nm laser (1 W cm^{-2}, 1.5 min). The fluorescence signals of both groups of cells after 8, 24 and 48 h incubation were then recorded.

Photothermal ablation of cancer cells

The photothermal therapeutic effect of DACF on 4T1 cells was characterized *in vitro* through live/dead assays, in which 4T1 cells were incubated with DACF probes followed by 405 nm laser irradiation (denoted as DACF + 405 nm), 4T1 cells receiving physiological saline (denoted as control), receiving DACF and 808 nm laser irradiation (denoted as DACF + 808 nm), and receiving DACF, 405 nm and 808 nm laser irradiation (denoted as DACF + 405 nm + 808 nm) were designed. The exposure time for the 405 nm laser (1 W cm^{-2}) and then the 808 nm laser (3 W cm^{-2}) was 1.5 min and 2 min. The cells receiving different combination treatments were stained with the live/dead staining kit and observed with a fluorescence microscope (OLYMPUS, IX73). The living cells appeared green, while the dead ones were red. The photothermal ablation effect of DACF was further evaluated through MTT and apoptotic analysis using flow cytometry. 4T1 cells were planted in 96-well plates with a concentration of 5×10^3 cells per well. After growing for 24 h, they were subjected to different combination treatments as mentioned above and analyzed through MTT assay. In parallel, 4T1 cells were seeded into 12-well plates at a density of 8×10^4 cells per well. After growing for 24 h, they were subjected to different combination treatments as mentioned above. Typically, 24 h post treatment, the cells were collected and washed with PBS three times, and then dyed with an Annexin VPE/7-AAD apoptosis detection kit (BD Inc.). Finally, the cells were subjected to flow cytometry analysis.

Mice tumor model construction

All animal experiments were conducted according to the Guidelines for the Care and Use of Laboratory Animals of Soochow University and were approved by the Animal Ethics Committee of the Soochow University Laboratory Animal Center (Suzhou, China). The 4T1 tumor models were generated by subcutaneous injection of 1×10^6 cells in 50 μL of PBS into the flank region of the left and right back of 5 week old female nude mice (for NIRF and PA imaging) or the flank region of the right back of 5 week old female BALB/c mice (for PTT treatment). Mice were selected for imaging and therapeutic experiments when their tumors grew to 50 mm^3. All animal experiment protocols were compliant with the Animal Ethics Committee of the Soochow University Laboratory Animal Center.

In vivo fluorescence imaging of tumors

The nude mice bearing two 4T1 tumors were injected with 200 μL of DACF or CF (45 μM) *via* the tail vein. At 0.5 h post-injection, the left tumor was exposed to 405 nm laser light (1 W cm^{-2}) for 10 min. The mice were then anesthetized with 3% isoflurane mixed with oxygen gas (0.5 L min^{-1}) and imaged using an IVIS spectrum at different time points. NIR light with a central wavelength at 745 nm was used as the excitation source. *In vivo* spectral imaging from 790 to 840 nm (10 nm step) was carried out with an exposure time of 200 ms for each image frame. The fluorescence images were finally analyzed with vendor software to separate autofluorescence from chromophore signals through spectral unmixing algorithms.

Ex vivo biodistribution studies

For the *ex vivo* biodistribution study, mice were sacrificed at 24 h post-irradiation of 405 nm laser light (1 W cm^{-2}), and then the major organs and tumorous tissues were carefully harvested and rinsed with PBS buffer (pH = 7.4), placed on black paper, and immediately imaged with an IVIS spectrum. After that, the tumors were subsequently collected for cryosection and eventually imaged by using an FV1200 laser scanning confocal microscope.

In vivo photoacoustic imaging

The nude mice bearing two 4T1 tumors were injected with 200 μL of DACF (45 μM) through the tail vein. At 30 min post-injection, the left tumor was exposed to 405 nm laser light (1 W cm^{-2}) for 10 min. Subsequently, the mice were anesthetized with isoflurane, and placed into a water bath to maintain their body temperature at 37 °C for the subsequent tumor PA imaging performed with a Multispectral Optoacoustic Tomography scanner (MSOT) under excitation light of 680 nm at different time points. After imaging reconstruction, the probe signal in the tumor area was measured by ROI analysis using the MSOT imaging system software package.

In vivo photothermal therapy

The tumor-bearing BALB/c mice were divided into four groups (n = 5) and then subjected with different combination treatments, *i.e.*, intravenous injection of DACF followed by 405 nm irradiation (denoted as DACF + 405 nm), intravenous injection of DACF followed by 808 nm irradiation (denoted as DACF + 808 nm), and intravenous injection of DACF followed by both 405 nm and 808 nm irradiation (denoted as DACF + 405 nm + 808 nm), while mice receiving PBS served as the control. The exposure time for the 405 nm laser (1 W cm^{-2}) and then the 808 nm laser (1 W cm^{-2}) was 10 and 5 min, respectively. The real-time thermal images of the mice were recorded with an infrared thermal imaging camera (FLIR, A65) during treatment. The therapeutic effect could be clearly seen from the photographs of typical tumors extracted 30 days post treatment. The tumor size was measured with calipers every 2 days, and the tumor volume (V, mm^3) was calculated as $V = LW^2/2$, where L and W are the length and width of the tumor, respectively. The tumor tissues were resected from the mice 3 days post treatment for evaluating the therapeutic efficacy of different treatments through pathological analysis.

Histological analysis

The mice from the control or treated groups were sacrificed and the main organs, such as heart, liver, spleen, lungs, and

kidneys, were resected, fixed in 10% neutral buffered formalin, processed routinely into paraffin, sectioned at 5 microns, and stained with hematoxylin & eosin (H&E). The histology and morphology of slices were captured with a Leica microscope (DM750).

Data availability

Additional data and NMR spectra, mass spectra, in-gel analysis, cellular uptake, CLSM images, *in vivo* real-time tumor imaging, photothermal effect, biodistribution analysis, apoptosis rates, hyperthermia heating curves tumor images, body weight, H&E staining, blood routine and blood chemical analysis can be found in the ESI.†

Author contributions

R. S., Y. Z., X. C., and H. S. conceived and designed the project. R. S. and Y. Z. performed all experiments and wrote the draft manuscript. Y. G., A. W., M. Z. and J. Z. help to analyze and interpret the data. X. C., and H. S. revised the final manuscript. All authors discussed the results and contributed to the final manuscript.

Conflicts of interest

There are no conflicts to declare.

Acknowledgements

We acknowledge the financial support from the National Science Foundation of China (22077092 and 81902913), the Training Program of the Major Research Plan of the National Natural Science Foundation of China (91959123), the Natural Science Foundation of Jiangsu Province (BK20190821), the Open Project Program of the State Key Laboratory of Radiation Medicine and Protection (GZK1202132, GZK1202140, and GZK1202017) and a project funded by the Priority Academic Program Development of Jiangsu Higher Education Institutions.

Notes and references

1 A. Louie, Multimodality imaging probes: design and challenges, *Chem. Rev.*, 2010, **110**(5), 3146–3195.
2 B. R. Smith and S. S. Gambhir, Nanomaterials for *in vivo* imaging, *Chem. Rev.*, 2017, **117**(3), 901–986.
3 R. Weissleder, M. C. Schwaiger, S. S. Gambhir and H. Hricak, Imaging approaches to optimize molecular therapies, *Sci. Transl. Med.*, 2016, **8**(355), 355ps16.
4 H. W. Liu, L. L. Chen, C. Y. Xu, Z. Li, H. Y. Zhang, X. B. Zhang and W. H. Tan, Recent progress in the development of near-infrared fluorescent probes for bioimaging applications, *Chem. Soc. Rev.*, 2018, **47**(18), 7140–7180.
5 X. S. Li, J. Kim, J. Yoon and X. Y. Chen, Cancer-associated, stimuli-driven, turn on theranostics for multimodality imaging and therapy, *Adv. Mater.*, 2017, **29**(23), 1606857.
6 A. Razgulin, N. Ma and J. H. Rao, Strategies for *in vivo* imaging of enzyme activity: an overview and recent advances, *Chem. Soc. Rev.*, 2011, **40**(7), 4186–4216.
7 Y. Q. Zhang, J. Fang, S. Y. Ye, Y. Zhao, A. N. Wang, Q. L. Mao, C. X. Cui, Y. L. Feng, J. C. Li, S. N. Li, M. Y. Zhang and H. B. Shi, Hydrogen sulphide-responsive and depleting nanoplatform for cancer photodynamic therapy, *Nat. Commun.*, 2022, **13**(1), 1685.
8 J. C. Li and K. Y. Pu, Development of organic semiconducting materials for deep-tissue optical imaging, phototherapy and photoactivation, *Chem. Soc. Rev.*, 2019, **48**(1), 38–71.
9 R. Weissleder, C. H. Tung, U. Mahmood and A. Bogdanov, In vivo imaging of tumors with protease-activated near-infrared fluorescent probes, *Nat. Biotechnol.*, 1999, **17**(4), 375–378.
10 A. L. Alexander, H. Chen, K. Cheng, Y. Sun, G. S. Hong, C. R. Qu, S. Diao, Z. X. Deng, X. M. Hu, B. Zhang, X. D. Zhang, O. K. Yaghi, Z. R. Alamparambil, X. C. Hong, Z. Cheng and H. J. Dai, A small-molecule dye for NIR-II imaging, *Nat. Mater.*, 2015, **15**(2), 235–242.
11 X. Q. Meng, Y. T. Yang, L. H. Zhou, L. Zhang, Y. L. Lv, S. P. Li, Y. Y. Wu, M. B. Zheng, W. J. Li, G. H. Gao, G. J. Deng, T. Jiang, D. P. Ni, P. Gong and L. T. Cai, Dual-responsive molecular probe for tumor targeted imaging and photodynamic therapy, *Theranostics*, 2017, **7**(7), 1781–1794.
12 T. Myochin, K. Hanaoka, S. Iwaki, T. Ueno, T. Komatsu, T. Terai, T. Nagano and Y. Urano, Development of a series of near-infrared dark quenchers based on Si-rhodamines and their application to fluorescent probes, *J. Am. Chem. Soc.*, 2015, **137**(14), 4759–4765.
13 S. Y. Li, H. Cheng, B. R. Xie, W. X. Qiu, L. L. Song, R. X. Zhuo and X. Z. Zhang, A ratiometric theranostic probe for tumor targeting therapy and self-therapeutic monitoring, *Biomaterials*, 2016, **104**, 297–309.
14 L. Yin, H. Sun, H. Zhang, L. He, L. Qiu, J. G. Lin, H. W. Xia, Y. Q. Zhang, S. J. Ji, H. B. Shi and M. T. Gao, Quantitatively visualizing tumor-related protease activity *in vivo* Using a ratiometric photoacoustic probe, *J. Am. Chem. Soc.*, 2019, **141**(7), 3265–3273.
15 Y. Q. Wang, X. M. Hu, J. H. Weng, J. B. Li, Q. L. Fan, Y. Zhang and D. J. Ye, Photoacoustic imaging of tumor apoptosis *via* caspase-instructed macrocyclization and self-assembly, *Angew. Chem., Int. Ed.*, 2019, **58**(15), 4886–4890.
16 M. Ogawa, N. Kosaka, P. L. Choyke and H. Kobayashi, In vivo molecular imaging of cancer with a quenching near-infrared fluorescent probe using conjugates of monoclonal antibodies and indocyanine green, *Cancer Res.*, 2009, **69**(4), 1268–1272.
17 H. Yang, H. J. Mao, Z. H. Wan, A. J. Zhu, M. Guo, X. M. Li, J. L. Wan, X. L. Yang, X. T. Shuai and H. B. Chen, Micelles assembled with carbocyanine dyes for theranostic near-infrared fluorescent cancer imaging and photothermal therapy, *Biomaterials*, 2013, **34**(36), 9124–9133.
18 J. A. Carr, D. Franke, J. R. Caram, C. F. Perkinson, M. Saif, V. Askoxylakis, M. Datta, D. Fukumura, R. K. Jain, M. G. Bawendi and O. Bruns, Shortwave infrared fluorescence imaging with the clinically approved near-

infrared dye indocyanine green, *Proc. Natl. Acad. Sci. U. S. A.*, 2018, **15**(17), 4465–4470.

19 Y. Q. Zhang, M. Zhao, J. Fang, S. Y. Ye, A. N. Wang, Y. Zhao, C. X. Cui, L. He and H. B. Shi, Smart on-site immobilizable NIR-II fluorescent nanoprobes for ultra long-term imaging-guided tumor surgery and photothermal therapy, *ACS Appl. Mater. Interfaces*, 2021, **13**(11), 12857–12865.

20 S. Mura, J. Nicolas and P. Couvreur, Stimuli-responsive nanocarriers for drug delivery, *Nat. Mater.*, 2013, **12**(11), 991–1003.

21 J. F. Lovell, C. S. Jin, E. Huynh, H. Jin, C. Kim, J. L. Rubinstein, W. C. Chan, W. Cao, L. V. Wang and G. Zheng, Porphysome nanovesicles generated by porphyrin bilayers for use as multimodal biophotonic contrast agents, *Nat. Mater.*, 2011, **10**(4), 324–332.

22 J. C. Li, J. H. Rao and K. Y. Pu, Recent progress on semiconducting polymer nanoparticles for molecular imaging and cancer phototherapy, *Biomaterials*, 2018, **155**, 217–235.

23 M. Moros, B. Hernáez, E. Garet, J. T. Dias, B. Sáez, V. Grazú, Á. González-Fernández, C. Alonso and J. M. de la Fuente, Monosaccharides *versus* PEG-functionalized NPs: influence in the cellular uptake, *ACS Nano*, 2012, **6**(2), 1565–1577.

24 P. A. Wender, D. J. Mitchell, K. Pattabiraman, E. T. Pelkey, L. Steinman and J. B. Rothbard, The design, synthesis, and evaluation of molecules that enable or enhance cellular uptake: peptoid molecular transporters, *Proc. Natl. Acad. Sci. U. S. A.*, 2000, **97**(24), 13003–13008.

25 C. E. Ashley, E. C. Carnes, G. K. Phillips, D. Padilla, P. N. Durfee, P. A. Brown, T. N. Hanna, J. Liu, B. Phillips, M. B. Carter, N. J. Carroll, X. Jiang, D. R. Dunphy, C. L. Willman, D. N. Petsev, D. G. Evans, A. N. Parikh, B. Chackerian, W. Wharton, D. S. Peabody and C. J. Brinker, The targeted delivery of multicomponent cargos to cancer cells by nanoporous particle-supported lipid bilayers, *Nat. Mater.*, 2011, **10**(5), 389–397.

26 A. N. Wang, J. Fang, S. Y. Ye, Q. L. Mao, Y. Zhao, C. X. Cui, Y. Q. Zhang, Y. L. Feng, J. C. Li, L. He, L. Qiu and H. B. Shi, Assembly Transformation Jointly Driven by the LAP Enzyme and GSH Boosting Theranostic Capability for Effective Tumor Therapy, *ACS Appl. Mater. Interfaces*, 2021, **13**(50), 59787–59802.

27 Y. Bae, S. Fukushima, A. Harada and K. Kataoka, Design of environment-sensitive supramolecular assemblies for intracellular drug delivery: polymeric micelles that are responsive to intracellular pH change, *Angew. Chem., Int. Ed.*, 2003, **42**(38), 4640–4643.

28 S. Wang, P. Huang and X. Y. Chen, Hierarchical targeting strategy for enhanced tumor tissue accumulation/retention and cellular internalization, *Adv. Mater.*, 2016, **28**(34), 7340–7364.

29 H. B. Shi, R. T. K. Kwok, J. Liu, B. Xing, B. Z. Tang and B. Liu, Real-time monitoring of cell apoptosis and drug screening using fluorescent light-up probe with aggregation-induced emission characteristics, *J. Am. Chem. Soc.*, 2012, **134**(43), 17972–17981.

30 Y. Ding, Y. Kang and X. Zhang, Enzyme-responsive polymer assemblies constructed through covalent synthesis and supramolecular strategy, *Chem. Commun.*, 2015, **51**(6), 996–1003.

31 R. C. Qian, L. Ding, L. W. Yan, M. F. Lin and H. X. Ju, A robust probe for lighting up intracellular telomerase *via* primer extension to open a nicked molecular beacon, *J. Am. Chem. Soc.*, 2014, **136**(23), 8205–8208.

32 A. N. Wang, L. Yin, L. He, H. W. Xia, F. Chen, M. Zhao, J. N. Ding and H. B. Shi, An acidic pH/reduction dual-stimuli responsive nanoprobe for enhanced CT imaging of tumours in vivo, *Nanoscale*, 2018, **10**(43), 20126–20130.

33 C. H. Ren, J. W. Zhang, M. S. Chen and Z. M. Yang, Self-assembling small molecules for the detection of important analytes, *Chem. Soc. Rev.*, 2014, **43**(21), 7257–7266.

34 Y. Gao, J. F. Shi, D. Yuan and B. Xu, Imaging enzyme-triggered self-assembly of small molecules inside live cells, *Nat. Commun.*, 2012, **3**(1), 1033.

35 Z. Feng, H. M. Wang and B. Xu, Instructed-assembly of peptides for intracellular enzyme sequestration, *J. Am. Chem. Soc.*, 2018, **140**(48), 16433–16437.

36 G. L. Liang, H. J. Ren and J. H. Rao, A biocompatible condensation reaction for controlled assembly of nanostructures in living cells, *Nat. Chem.*, 2010, **2**(3), 54–60.

37 D. J. Ye, A. J. Shuhendler, L. Cui, S. T. Sui, G. Tikhomirov, D. W. Felsher and J. H. Rao, Bioorthogonal cyclization-mediated *in situ* self-assembly of small-molecule probes for imaging caspase activity in vivo, *Nat. Chem.*, 2014, **6**(6), 519–526.

38 A. Dragulescu-Andrasi, S. R. Kothapalli, G. A. Tikhomirov, J. H. Rao and S. S. Gambhir, Activatable oligomerizable imaging agents for photoacoustic imaging of furin-like activity in living subjects, *J. Am. Chem. Soc.*, 2013, **135**(30), 11015–11022.

39 Z. J. Hai, J. D. Li, J. J. Wu, J. C. Xu and G. L. Liang, Alkaline phosphatase-triggered simultaneous hydrogelation and chemiluminescence, *J. Am. Chem. Soc.*, 2017, **139**(3), 1041–1044.

40 Z. Zheng, P. Y. Chen, M. L. Xie, C. F. Wu, Y. F. Luo, W. T. Wang, J. Jiang and G. L. Liang, Cell environment-differentiated self-assembly of nanofibers, *J. Am. Chem. Soc.*, 2016, **138**(35), 11128–11131.

41 D. B. Cheng, D. Wang, Y. J. Gao, L. Wang, Z. Y. Qiao and H. Wang, Autocatalytic morphology transformation platform for targeted drug accumulation, *J. Am. Chem. Soc.*, 2019, **141**(10), 4406–4411.

42 D. B. Cheng, X. H. Zhang, Y. J. Gao, L. Ji, D. Y. Hou, Z. Q. Wang, W. H. Xu, Z. Y. Qiao and H. Wang, Endogenous reactive oxygen species-triggered morphology transformation for enhanced cooperative interaction with mitochondria, *J. Am. Chem. Soc.*, 2019, **141**(18), 7235–7239.

43 D. Zhang, G. B. Qi, Y. X. Zhao, S. L. Qiao, C. Yang and H. Wang, In situ formation of nanofibers from purpurin18-peptide conjugates and the assembly induced retention effect in tumor sites, *Adv. Mater.*, 2015, **27**(40), 6125–6130.

44 P. P. He, X. D. Li, L. Wang and H. Wang, Bispyrene-based self-assembled nanomaterials: *in vivo* self-assembly,

transformation, and biomedical effects, *Acc. Chem. Res.*, 2019, **52**(2), 367–378.

45 M. H. Lee, N. Park, C. Yi, J. H. Han, J. H. Hong, K. P. Kim, D. H. Kang, J. L. Sessler, C. Kang and J. S. Kim, Mitochondria-immobilized pH-sensitive off–on fluorescent probe, *J. Am. Chem. Soc.*, 2014, **136**(40), 14136–14142.

46 G. L. Ke, Z. Zhu, W. Wang, Y. Zou, Z. C. Guan, S. S. Jia, X. M. Wu and C. Y. Yang, A cell-surface-anchored ratiometric fluorescent probe for extracellular pH sensing, *ACS Appl. Mater. Interfaces*, 2014, **6**(17), 15329–15334.

47 M. Y. Xiong, H. J. Zhu, Q. M. Rong, C. Yang, L. P. Qiu, X. B. Zhang and W. H. Tan, A membrane-anchored fluorescent probe for detecting K^+ in the cell microenvironment, *Chem. Commun.*, 2016, **52**(25), 4679–4682.

48 S. Xu, H. W. Liu, X. Yin, L. Yuan, S. Y. Huan and X. B. Zhang, A cell membrane-anchored fluorescent probe for monitoring carbon monoxide release from living Cells, *Chem. Sci.*, 2019, **10**(1), 320–325.

49 C. Jin, J. X. He, J. M. Zou, W. J. Xuan, T. Fu, R. W. Wang and W. H. Tan, Phosphorylated lipid-conjugated oligonucleotide selectively anchors on cell membranes with high alkaline phosphatase expression, *Nat. Commun.*, 2019, **10**(1), 2704.

50 T. Temma, H. Hanaoka, A. Yonezawa, N. Kondo, K. Sano, T. Sakamoto, M. Seiki, M. Ono and H. Saji, Investigation of a MMP-2 activity-dependent anchoring probe for nuclear imaging of cancer, *PLoS One*, 2014, **9**(7), e102180.

51 R. Tong, H. H. Chiang and D. S. Kohane, Photoswitchable nanoparticles for *in vivo* cancer chemotherapy, *Proc. Natl. Acad. Sci. U. S. A.*, 2013, **110**(47), 19048–19053.

52 X. Z. Ai, J. Mu and B. G. Xing, Recent advances of light-mediated theranostics, *Theranostics*, 2016, **6**(11), 1899–1917.

53 X. J. Cheng, R. Sun, L. Yin, Z. F. Chai, H. Shi and M. Y. Gao, Light-triggered assembly of gold nanoparticles for photothermal therapy and photoacoustic imaging of tumors in vivo, *Adv. Mater.*, 2017, **29**(6), 201604894.

54 G. W. Preston and A. J. Wilson, Photo-induced covalent cross-linking for the analysis of biomolecular interactions, *Chem. Soc. Rev.*, 2013, **42**(8), 3289–3301.

55 H. B. Shi, C. J. Zhang, G. Y. Chen and S. Q. Yao, Cell-based proteome profiling of potential dasatinib targets by use of affinity-based probes, *J. Am. Chem. Soc.*, 2012, **134**(6), 3001–3014.

56 Z. Q. Li, D. Y. Wang, L. Li, S. J. Pan, Z. K. Na, C. Y. Tan and S. Q. Yao, Minimalist cyclopropene-containing photo-cross-linkers suitable for live-cell imaging and affinity-based protein labeling, *J. Am. Chem. Soc.*, 2014, **136**(28), 9990–9998.

57 Y. Yang, H. P. Song, D. He, S. Zhang, S. Z. Dai, S. X. Lin, R. Meng, C. Wang and P. Chen, Genetically encoded protein photocrosslinker with a transferable mass spectrometry-identifiable label, *Nat. Commun.*, 2016, **7**, 12299.

58 S. Y. Ye, C. X. Cui, X. J. Cheng, M. Zhao, Q. L. Mao, Y. Q. Zhang, A. N. Wang, J. Fang, Y. Zhao and H. B. Shi, Red light-initiated crosslinking of NIR probes to cytoplasmic RNA: an innovative strategy for prolonged imaging and unexpected tumor suppression, *J. Am. Chem. Soc.*, 2020, **92**(24), 16113–16121.

59 L. Liu, M. H. Engelhard and M. D. Yan, Surface and Interface Control on Photochemically Initiated Immobilization, *J. Am. Chem. Soc.*, 2006, **128**(43), 14067–14072.

60 R. Sun, L. Yin, S. H. Zhang, L. He, X. J. Cheng, A. N. Wang, H. W. Xia and H. B. Shi, Simple light-triggered fluorescent labeling of silica nanoparticles for cellular imaging applications, *Chem. - Eur. J.*, 2017, **23**(56), 13893–13896.

61 Q. L. Mao, J. Fang, A. N. Wang, Y. Q. Zhang, C. X. Cui, S. Y. Ye, Y. Zhao, Y. L. Feng, J. C. Li and H. B. Shi, Aggregation of gold nanoparticles triggered by hydrogen peroxide-initiated chemiluminescence for activated tumor theranostics, *Angew. Chem., Int. Ed.*, 2021, **60**(44), 23805–23811.

62 J. Fang, Y. L. Feng, Y. Q. Zhang, A. N. Wang, J. C. Li, C. X. Cui, Y. R. Guo, J. F. Zhu, Z. Z. Lv, Z. S. Zhao, C. J. Xu and H. B. Shi, An Alkaline Phosphatase-Controllable and Red Light-Activated RNA Modification Approach for Precise Tumor Suppression, *J. Am. Chem. Soc.*, 2022, **144**, 23061–23072.

63 S. Y. Ye, C. X. Cui, X. J. Cheng, M. Zhao, Q. L. Mao, Y. Q. Zhang, A. N. Wang, J. Fang, Y. Zhao and H. B. Shi, Red Light-initiated Crosslinking of NIR Probes to Cytoplasmic RNA: An Innovative Strategy for Prolonged Imaging and Unexpected Tumor Suppression, *J. Am. Chem. Soc.*, 2020, **142**(51), 21502–21512.

64 S. Y. Dai and D. Yang, A Visible and Near-Infrared Light Activatable diazocoumarin probe for fluorogenic protein labeling in living cells, *J. Am. Chem. Soc.*, 2020, **142**(40), 17156–17166.

65 U. K. Shigdel, J. L. Zhang and C. He, Diazirine-based DNA photo-cross-linking probes for the study of protein DNA inter-actions, *Angew. Chem., Int. Ed.*, 2008, **47**(1), 90–93.

66 Z. Q. Li, P. L. Hao, L. Li, C. Y. J. Tan, X. M. Cheng, G. Y. J. Chen, S. K. Sze, H. M. Shen and S. Q. Yao, Design and synthesis of minimalist terminal alkyne-containing diazirine photo-crosslinkers and their incorporation into kinase inhibitors for cell- and tissue-based proteome profiling, *Angew. Chem., Int. Ed.*, 2013, **52**(33), 8551–8556.